*J. Fluid Mech.* (2008), *vol.* 615, *pp.* 211–220.  
doi:10.1017/S0022112008003583 Printed in the United Kingdom

# Effects of three-dimensionality on thrust production by a pitching panel

MELISSA A. GREEN AND ALEXANDER J. SMITS

Department of Mechanical and Aerospace Engineering, Princeton University, Princeton, NJ 08544, USA

(Received 9 April 2008 and in revised form 4 August 2008)

To understand the fluid dynamics of a biologically inspired unsteady low-aspect-ratio propulsor, unsteady pressure distributions were measured and compared with time-averaged thrust performance and wake visualizations. The experiments were performed on rigid rectangular panels with different aspect ratios, pitching in a uniform flow. Panel aspect ratio and pitching amplitude were shown to affect the magnitude and time dependence of the pressure distribution on the panel surface, the vorticity generation on the panel, and thrust production. A new scaling is proposed that includes these parameters and collapses the oscillating pressure magnitude and the thrust coefficient.

## 1. Introduction

The locomotion of fish and aquatic animals is achieved by the oscillation of fins and flukes, which creates highly three-dimensional, unsteady flow fields that are not yet well-understood. Two-dimensional foils, when efficiently producing thrust, have been observed to generate two spanwise vortices at the trailing edge during each flapping cycle, referred to as a 2-S wake (Koochesfahani 1989; Williamson & Roshko 1988). These vortices are arranged in a reverse von Kármán vortex street, and the principal non-dimensional parameter is the Strouhal number,

$$St = fA/U. \tag{1.1}$$

Here, $f$ is the frequency of oscillation, $A$ is the width of the wake, and $U$ is the free-stream velocity. The peak-to-peak amplitude of the trailing edge is commonly used as an approximation for $A$. Triantafyllou, Triantafyllou & Grosenbaugh (1993) used a linear stability analysis on the wake of an oscillating foil to show that predicted optimal efficiency for flapping foils occurs in the range $0.25 \leqslant St \leqslant 0.35$, and this was confirmed with a two-dimensional flapping foil experiment. Furthermore, analysis of the locomotion of a variety of fish species showed that many marine animals swim in this Strouhal number range.

Experiments and computations on pitching and flapping bodies of finite aspect ratio have revealed that the wake structure is considerably more complex than the two-dimensional case, and that it is a strong function of Strouhal number and aspect ratio $AR$ ($= S/C$, where $S$ is the span and $C$ is the chord). See, for example, von Ellenrieder, Parker & Soria (2003); Guglielmini (2004); Dong *et al.* (2005); Ghovardhan & Williamson (2005); Sarkar & Venkatraman (2006) and Borazjani & Sotiropoulos (2008). In particular, Buchholz & Smits (2008) performed wake studies and thrust measurements on a series of low-aspect-ratio rectangular pitching panels. At low Strouhal number, the 2-S structure was present in the wake, but as the

| Panel | Chord ($C$) | Span ($S$) | Aspect ratio ($AR = S/C$) | $A$ (mm) | $St$ | $Re = UC/\nu$ |
|---|---|---|---|---|---|---|
| 1 | 120 mm | 65 mm | 0.54 | 20 | 0.133–1.33 | 3500–35 000 |
| 1 | 120 mm | 65 mm | 0.54 | 40 | 0.222–2.67 | 3500–43 200 |
| 2 | 120 mm | 270 mm | 2.25 | 20 | 0.167–1.33 | 3500–28 800 |

TABLE 1. Summary of experimental parameters.

Strouhal number increased the wake bifurcated into a 2-P structure, in which two pairs of oppositely signed vortices are shed each pitching cycle. Additionally, for the same $St$, thrust was shown to increase with increasing aspect ratio, while a weaker inverse relationship was observed with pitching amplitude. They proposed that the appropriate additional scaling parameter for the effect of three-dimensionality is the ratio of amplitude to span $A/S$.

Here, we investigate the effects of three-dimensionality further by studying the unsteady pressure distributions on low-aspect-ratio rectangular pitching panels in order to describe the forces on the panel surface. Such measurements do not seem to be available, although Hilaire & Carta (1983) performed a survey of pressure experiments on an oscillating NACA 0012 airfoil to explore the effects of sweep angle and mean angle of attack. The focus of their work was the separation at the leading edge of the airfoil, and not the unsteady forces on it. In the area of experimental biology, Usherwood *et al.* (2005) performed pressure measurements on flapping pigeon wings by attaching transducers to the wings of flying pigeons. Other pressure measurements and calculations have been conducted on airfoils to investigate the effects of flutter (Singh, Aikat & Basu 1989; Ardonceau 1989), but the behaviour of the unsteady pressure and its relationship to thrust production has received little attention. From our results we propose a new scaling parameter to collapse the effects of three-dimensionality in the pressure distribution and the thrust coefficient.

## 2. Experimental apparatus

Pressure measurements were taken on the surface of rigid rectangular panels pitching about the leading edge in a uniform flow. Two aspect ratios ($AR$) were used (see table 1), where the higher-aspect-ratio panel spanned the water depth. The panels were clear acrylic with a thickness of 2 mm. They were supported at their leading edge by a shaft attached to a symmetric airfoil fairing based on a NACA 0012-64 airfoil, as described by Buchholz & Smits (2008), to inhibit leading-edge separation and the formation of the dynamic stall vortex. The actuation of the panel used the same mechanism as this previous work, which achieved the pitching motion by using a four-bar linkage driven by a d.c. servomotor. The panel and fairing were mounted vertically in a water channel of width 0.46 m and depth 0.29 m, with the panel midspan positioned at a depth halfway between the top and bottom of the channel, as shown in figure 1. An acrylic plate, 12 mm thick and 1.22 m long, was used to close the free surface to prevent the formation of surface waves. Any effect of the gaps between the edge of the panel and the top surface plate and bottom wall were checked by varying the gap size. Decreasing it to 5 mm at the top and bottom edges showed no change in the pressure at midspan.

The pressure was measured using a Validyne DP-15 differential pressure transducer and CD379 carrier demodulator. The pressure transducer had a range of 3.5–5.5 in.

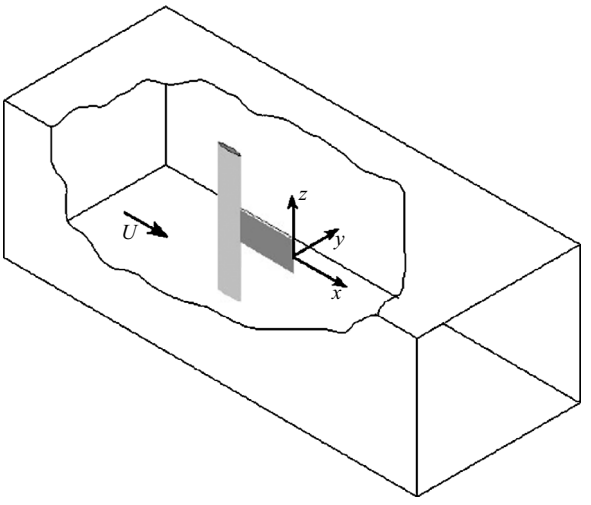


FIGURE 1. Panel and fairing position in water channel test section.

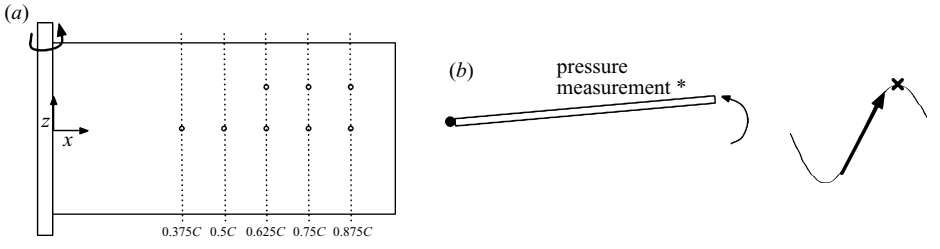


FIGURE 2. (*a*) Pressure port placement on the low-aspect-ratio ($S/C = 0.54$) Panel 1. (b) Schematic of the panel advancing, and its associated trailing-edge amplitude curve.

of water, with an accuracy of $\pm 0.25\%$ of full range. Five 3.2 mm diameter pressure ports were placed along the mid-span of each panel. For the low-aspect-ratio panel (Panel 1), three additional pressure ports were placed off the midspan, a quarter-span length away from the edge of the panel; their chordwise locations coincided with the three centreline ports closest to the trailing edge, as shown in figure 2. A schematic of the panel in advancing motion (toward the measurement surface) and its associated motion curve, which will be used in § 3.1, is also shown. The transducer was connected to the pressure ports by tubing approximately 115 cm long.

Experiments were conducted for a range of Strouhal numbers at moderate Reynolds numbers, as given in table 1; the velocity was varied from 0.03 to 0.3 m s$^{-1}$. Measurements were obtained for the low-aspect-ratio Panel 1 pitching at peak-to-peak amplitudes $A = 20$ and 40 mm and for the high-aspect-ratio Panel 2 at $A = 20$ mm.

The pressure was measured using one port location at a time until the entire distribution was obtained. The phase of the panel motion was monitored using an optical encoder, and the pressure distributions were phase averaged to smooth the data. A typical phase-averaged pressure deviation from the time-averaged mean is shown in figure 3. The error bars represent the composite errors (added in quadrature) arising from the limited frequency response of the system and the effects of phase-averaging. To determine the frequency response of the system, a dynamic calibration of the transducer was performed using a step input. The transducer and the pressure

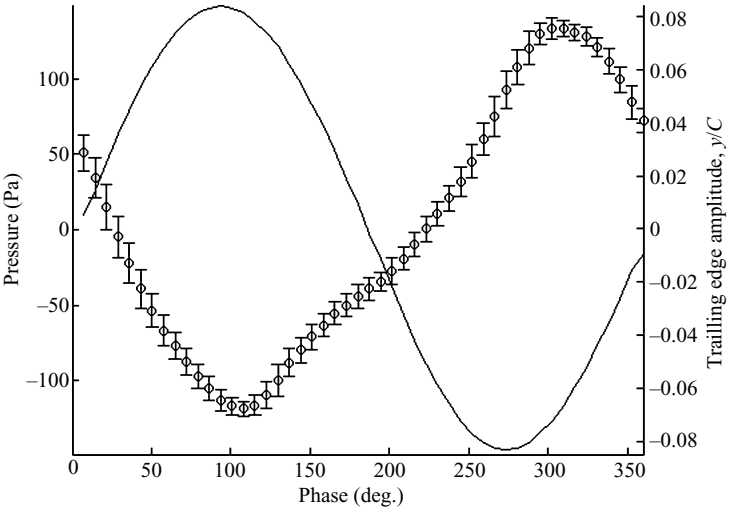


FIGURE 3. Unsteady pressure variation at $0.875C$ on Panel 1, $A = 20\,\text{mm}$, $St = 0.27$. —, Trailing-edge amplitude; ○, pressure deviation from the time-averaged mean.

tubing were modelled as a combination of second-order systems. It was found that the resonant frequency of the system was well above the pitching frequencies investigated. The error of the dynamic response was less than 5% for frequencies up to 3.9 Hz. At a pitching frequency of 2.67 Hz, the highest used for the present results, the error of was less than 2.3%. Most of the experiments were conducted at a frequency of 2 Hz, with a dynamic response error of 1.25%. The error at each point of the cycle due to phase-averaging was estimated to be two standard deviations based on the spread of points being averaged.

## 3. Results

### 3.1. *Pressure signals*

Consider the phase-averaged pressure trace obtained on the centreline at $0.875C$ on Panel 1 at $St = 0.27$ shown in figure 3, which Buchholz & Smits (2008) found to correspond closely to the most efficient level of thrust production. The pressure reaches its minimum at a phase of $\phi \approx 100°$, shortly after the panel measurement surface stops advancing ($\phi = 90°$). Similarly, the pressure maximum occurs at a phase of $\phi \approx 300°$, approximately one half-cycle later. The pressure minimum coincides almost exactly with the maximum panel acceleration in retreating motion, and while the pressure maximum is more delayed, it still coincides closely with the maximum panel acceleration in advancing motion.

As the panel retreats, the pressure rises quickly, then levels off for a short period before continuing to increase. This short plateau is attributed to spanwise flow from the edges relieving the low pressure along the midspan. As will be explained in § 3.2, a strong favourable pressure gradient acts toward the midspan during this time ($\phi \approx 135°$), which causes the subsequent loss of low pressure. Similar pressure signals were observed on the wings of pigeons during flight by Usherwood *et al.* (2005), who associated this plateau with the 'clap' of the wing, a 'period of high acceleration and relatively low differential pressure'. In the present measurements, this plateau in the pressure trace is seen for all Strouhal numbers at which the experiments were performed.

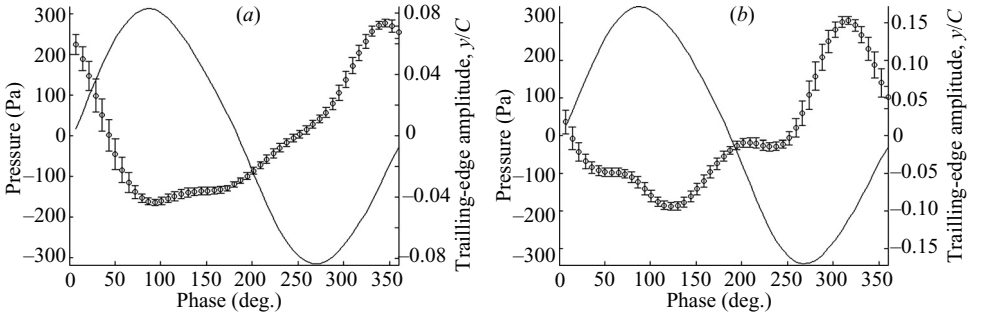


FIGURE 4. Unsteady pressure variation at $0.875C$ on (*a*) Panel 2, $A = 20$ mm, $St = 0.33$, and (*b*) Panel 1, $A = 40$ mm, $St = 0.33$. ——, Trailing-edge amplitude; ○, pressure deviation from the time-averaged mean.

Figure 4(*a*) shows the pressure variation at the same location and amplitude of motion on Panel 2 at $St = 0.33$ (corresponding to the highest efficiency for these conditions according to Buchholz & Smits 2008). For this higher-aspect-ratio panel, the pressure signal displays a larger trough that begins as the panel starts to pitch away and ends as it almost reaches its opposite extremum. The period of low pressure is more extended because the larger aspect ratio inhibits inflow from the spanwise edges which would tend to equalize the pressures.

Figure 4(*b*) shows the pressure variation at the same location on Panel 1, with $A = 40$ mm and $St = 0.33$ (again, this corresponds to the most efficient motion for this amplitude according to Buchholz & Smits 2008). There is a loss of low pressure as the panel retreats, as before, but an additional period of pressure loss appears as the panel motion reaches its maximum pitch angle ($\phi = 90°$). The increased pitching amplitude increases three-dimensional effects, which lead to additional low pressure losses.

### 3.2. *Pressure distributions*

The streamwise distribution of pressure on the advancing surface of Panel 1 pitching at $St = 0.27$ is shown in figure 5 for four phases of its motion, with the corresponding panel position and port locations superimposed. As the panel advances through zero angle of attack ($\phi = 0°$), an adverse pressure gradient is present along its midspan. When it reaches the extremum ($\phi = 90°$), the streamwise gradient on the top surface has changed, with strong favourable gradients near $x = 0.5C$ and $0.75C$, where $x$ is measured from the leading edge of the panel. A slight favourable pressure gradient persists as the panel retreats through the zero angle of attack ($\phi = 180°$). The pressure along the midspan then increases until the panel reaches the opposite extremum ($\phi = 270°$) with relatively strong adverse gradients again present near $x = 0.5C$ and $0.75C$. Similar streamwise distributions were observed for the higher aspect ratio and higher amplitude configurations.

The spanwise distribution of pressure on Panel 1 was measured at $0.875C$. A strong favourable gradient acting toward the midspan is observed as it is retreating ($\phi \approx 135°$), with the pressure magnitude at $z = 0.25S$ 47% higher than that at the midspan where $z = 0$. As a result, flow is induced from the advancing surface over the spanwise edges onto the retreating surface. It is this spanwise pressure gradient that relieves the period of low pressure on Panel 1. Half a cycle later, a favourable gradient is directed toward the spanwise edges of the panel on the now advancing surface, and the pressure at $z = 0.25S$ is only 60% of its value at the midspan. At this phase, fluid tends to flow away from the midspan upstream of the trailing edge.

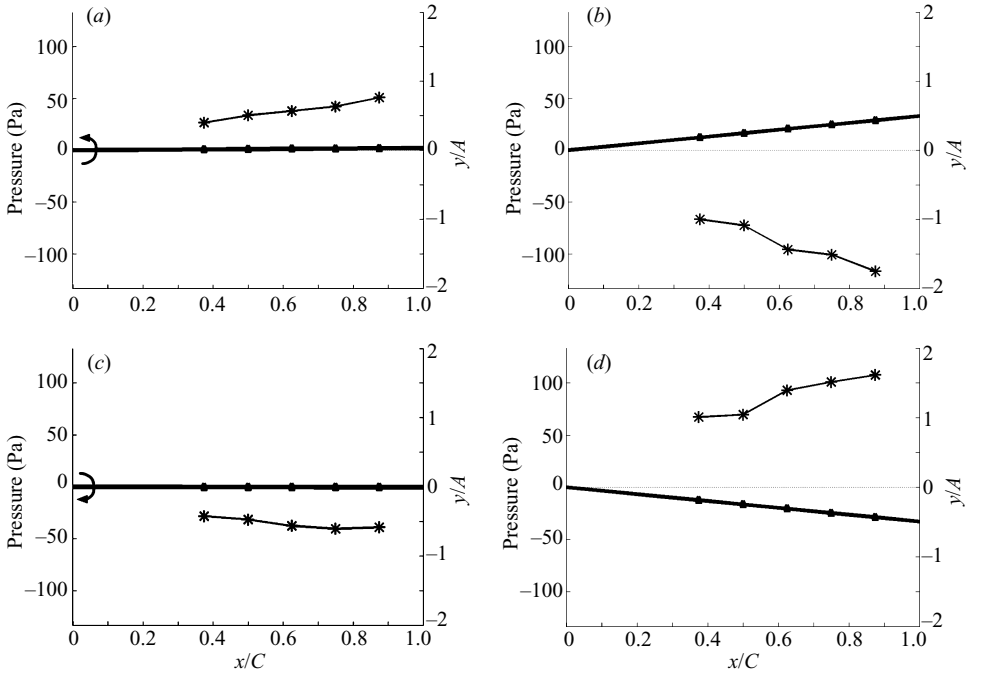


FIGURE 5. Streamwise distribution of pressure along the midspan for Panel 1 pitching at $St = 0.27$ and $A = 20$ mm. (*a*) $\phi = 0°$; (*b*) 90°; (*c*) 180°; (*d*) 270°. *, Pressure deviation from the time-averaged mean; black triangle, location of pressure port along the panel.

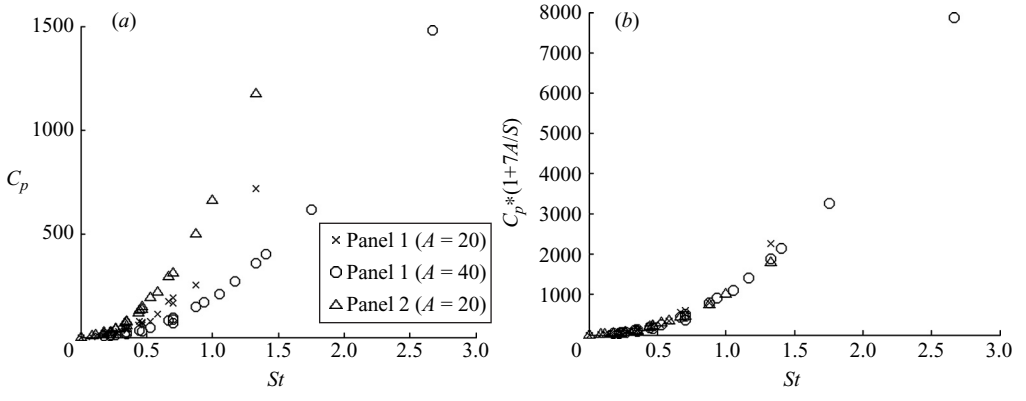


FIGURE 6. Peak to peak pressure amplitude at $x = 0.875C$: (*a*) $C_p$; (*b*) $C_p^*$.

### 3.3. *Scaling*

The coefficient of pressure $C_p$ is shown in figure 6(*a*) at $x = 0.875C$, where

$$C_p = \Delta p / \left(\tfrac{1}{2}\rho U^2\right), \tag{3.1}$$

and $\Delta p$ is the peak-to-peak amplitude of the pressure variation. The pressure coefficient follows distinct trends for each of the three experimental configurations. Buchholz & Smits (2008) showed that the thrust produced by pitching rigid rectangular panels depends on the Strouhal number and the aspect ratio $S/C$; also,

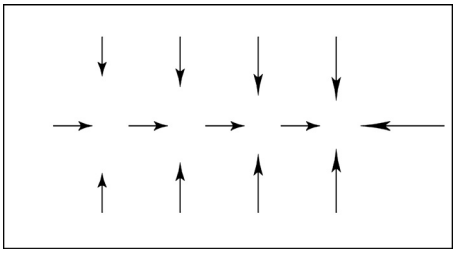

FIGURE 7. Pressure gradient and magnitude on advancing surface of panel inferred by Buchholz (2006). Flow is from left to right.

they showed a weak inverse relationship with the amplitude of oscillation $A$. Here we find that that the peak-to-peak amplitude of the oscillating pressure signal varies with aspect ratio and the ratio of pitching amplitude to chord, $A/C$. This suggests a new scaling:

$$C_p^* = C_p \left(1 + f\left(\frac{S}{C}, \frac{A}{C}\right)\right). \tag{3.2}$$

A simple form of $f$ taken as $f(x, y) \propto y/x$ leads to

$$C_p^* = C_p \left(1 + C_1 \frac{A}{S}\right). \tag{3.3}$$

As shown in figure 6($b$), the new scaling neatly collapses the pressure coefficient data. Note that as the aspect ratio goes to infinity, $C_p^* = C_p$, as required. This scaling is similar to the that used to account for the effects of aspect ratio on the lift coefficient in finite wing theory.

## 4. Discussion and conclusions

The pressure measurements along the midspan showed that the maximum and minimum pressures were associated with the extrema of the panel acceleration. When the panel motion reached an extremum, a positive streamwise pressure gradient existed along the surface that is beginning to advance, which is in contrast to steady flow at the same angle of incidence where a negative pressure gradient would be expected.

Buchholz (2006) used flow visualization and vorticity contours to infer the direction and relative magnitude of the pressure gradient on the advancing surface of the panel, as shown in figure 7. The measurements presented here confirm that a strong favourable streamwise gradient occurs over the region close to the trailing edge ($0.8 < x/C < 1$), but this pressure gradient continues to exert its influence as the panel stops and begins to move in the opposite direction.

The pressure signal reported here deviated from a smooth sinusoid during periods of low pressure, suggesting the presence of strong three-dimensional effects. Flow visualizations by Buchholz & Smits (2008) showed spanwise ejections of fluid at the phase where a strong favourable pressure gradient acts towards the spanwise edges. A strong spanwise adverse gradient was shown to exist half a cycle later, indicating flow toward the midspan of the panel. This low-aspect-ratio effect also explains the loss of low pressure along the midspan ports.

A new pressure coefficient $C_p^*$ that included the effects of aspect ratio and oscillation amplitude successfully collapsed the pressure results. Since the pressure distribution is directly related to the thrust $T$ produced by the panel, the following scaling is

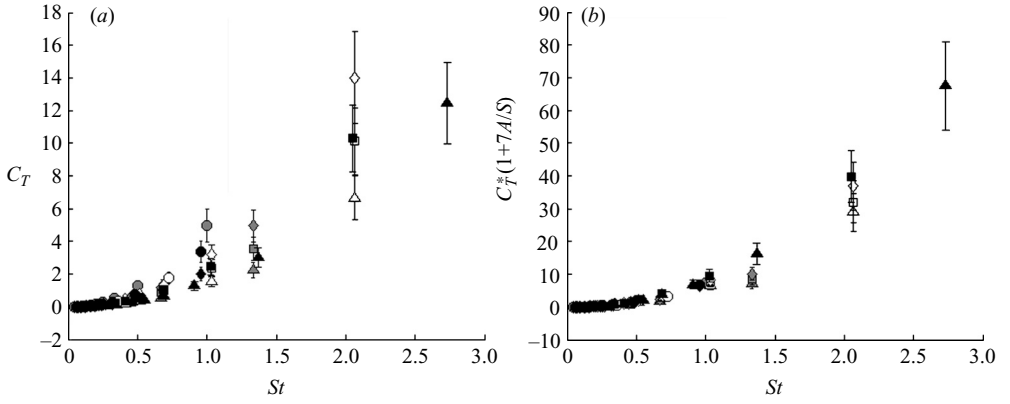


FIGURE 8. Thrust coefficient measured by Buchholz & Smits (2008). (*a*) $C_T$; (*b*) $C_T^*$ with $C_2 = 7$. Symbols refer to different panels and amplitudes.

suggested for the thrust coefficient $C_T$:

$$C_T^* = C_T \left(1 + C_2 \frac{A}{S}\right), \tag{4.1}$$

where

$$C_T = \frac{T}{\frac{1}{2}\rho U^2 SC}, \tag{4.2}$$

and $T$ is the resultant force in the streamwise direction. Mean thrust measurements on these panels were reported by Buchholz & Smits (2008). Figure 8(*a*, *b*) demonstrates that this scaling indeed collapses the thrust results within the uncertainty limits, and, the constant used to scale both the pressure and thrust data is the same: $C_1 = C_2 = 7$. Additional experiments with panels of varying chord are needed to generalize the proposed scaling.

By considering the aspect ratio and pitching amplitude, a new interpretation can be given to the particle image velocimetry (PIV) results of Buchholz (2006). Figure 9 shows data for Panels 1 and 2 pitching with the same trailing-edge amplitude. In figure 9(*a*), Panel 2 is pitching at $St = 0.36$ and the wake has a 2-S structure, with two single vortices being shed each flapping cycle. Panel 1, pitching at $St = 0.26$ (figure 9*b*), exhibits a 2-P structure, with two pairs of vortices shed each cycle. Previous work has shown that the transition from a 2-S structure to a 2-P structure is associated with an increase in Strouhal number, but here the transition, which occurs at a lower Strouhal number, is probably due to the decrease in aspect ratio.

The phase-averaged pressure traces at $0.875C$ shown in figure 10 indicate that as the panel retreats from the measurement surface, the pressure on Panel 2 stays at or near its minimum value for a larger fraction of the pitching period than in the low-aspect-ratio or high-amplitude cases. The vorticity contours in figure 9 show that for Panel 1 the trailing-edge structure is at a lateral distance $y/C \approx -0.30$, but for Panel 2 at the same phase of motion it is closer to the edge at $y/C \approx -0.15$. The prolonged low pressure on Panel 2 may cause the structure to remain closer to the trailing edge as it moves across the wake, and hence delay the breakdown of the structures into a 2-P wake. Hultmark, Leftwich & Smits (2007) and Tytell & Lauder (2004) observed a 2-P configuration in the wakes of a robotic lamprey and American eel, respectively. They described the formation of the 2-P wake structure as a consequence of the segmentation of the shear layer being shed from the trailing

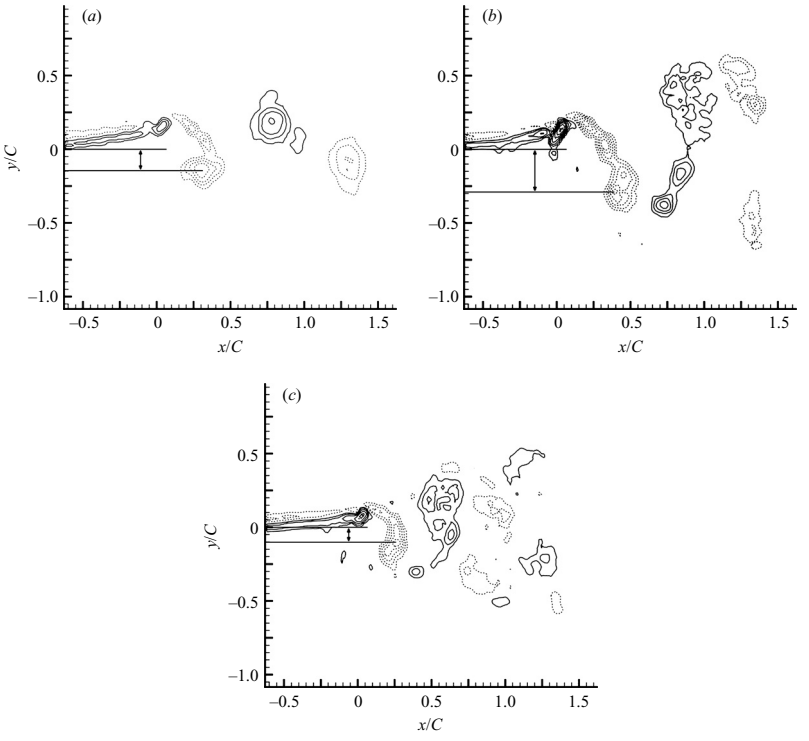


FIGURE 9. PIV results of Buchholz & Smits (2008) at the panel midspan at $\phi = 90°$: (*a*) Panel 2, $A = 31$ mm, $St = 0.36$, (*b*) Panel 1, $A = 31$ mm, $St = 0.26$, and (*c*) Panel 1, $A = 20$ mm and $St = 0.27$. Contour levels are $\pm n^2 s^{-1}$, $n = 2, 3, 4, \ldots, 10$.

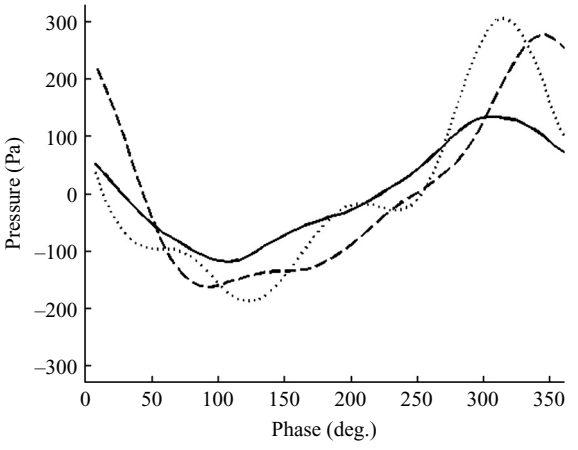


FIGURE 10. Unsteady pressure variation on the centreline at $0.875C$ with $A = 20$ mm and $St = 0.27$: ——, Panel 1, $A = 20$ mm; · · · ·, Panel 1, $A = 40$ mm; - - - -, Panel 2, $A = 20$ mm.

edge. If, as in the higher-aspect-ratio case presented here, the trailing-edge structure is pulled along with the panel surface, it will not spread into a shear layer and be susceptible to segmentation.

Similarly, an increase in pitching amplitude will enable the elongation and segmentation of the spanwise structure from the trailing edge when the panel is in a retreating motion. Figure 9(*c*) shows the wake of Panel 1 pitching at $A = 20$ mm

and $St = 0.27$. At $\phi = 90°$, the structure has travelled a shorter lateral distance than the same panel with a larger pitching amplitude ($A = 31$ mm), and it is located at $y/C \approx -0.10$, compared to $y/C \approx -0.30$ for the higher-amplitude case. The pressure traces shown in figure 10 indicate that when pitching with a higher amplitude, the panel experienced additional losses of low pressure. This loss of low pressure allows the trailing-edge structure to spread across the wake and break into two segments, forming the pairs that comprise the 2-P structure.

Previous work showed that an increase in unsteadiness, that is, an increase in $St$, caused the wake of rigid pitching propulsors to transition from the 2-S to the more complicated 2-P structure. The new scaling law for pressure and thrust results led to the inclusion of three-dimensional effects in the interpretation of the wake transition. The three-dimensionality increases when the aspect ratio of the panel decreases or when the pitching amplitude increases, and it is directly related to the time the shed vorticity dwells near the trailing edge. In this way, the qualitative wake characteristics are also consistent with the new scaling.

The authors wish to thank Dr James Buchholz for generously providing access to his data. This work was supported by NIH CNRS Grant 1R01NS054271.

## REFERENCES

Ardonceau, P. L. 1989 Unsteady pressure distribution over a pitching airfoil. *AIAA J.* **27**, 660–662.

Borazjani, I. & Sotiropoulos, F. 2008 Numerical investigation of the hydrodynamics of carangiform swimming in the transitional and inertial flow regimes. *J. Expl Biol.* (in press).

Buchholz, J. J. 2006 The flowfield and performance of a low aspect ratio unsteady propulsor. PhD thesis, Princeton University.

Buchholz, J. J. & Smits, A. J. 2008 The wake structure and thrust performance of a rigid low-aspect-ratio pitching panel. *J. Fluid Mech.* **603**, 331–365.

Dong, H., Mittal, R., Bozhurttas, M. & Najjar, F. 2005 Wake structure and performance of finite aspect-ratio flapping foils. *AIAA Paper* 2005-0081.

von Ellenrieder, K. D., Parker, K. & Soria, J. 2003 Flow structures behind a heaving and pitching finite-span wing. *J. Fluid Mech.* **490**, 129–138.

Ghovardhan, R. & Williamson, C. H. K. 2005 Vortex-induced vibrations of a sphere. *J. Fluid Mech.* **531**, 11–47.

Guglielmini, L. 2004 Modeling of thrust generating foils. PhD thesis, University of Genoa.

Hilaire, A. St & Carta, F. 1983 Analysis of unswept and swept wing chordwise pressure data from an oscillating NACA 0012 airfoil experiment. *NASA CR*-3567.

Hultmark, M., Leftwich, M. & Smits, A. J. 2007 Flowfield measurements in the wake of a robotic lamprey. *Exps. Fluids* **43**, 683–690.

Koochesfahani, M. M. 1989 Vortical patterns in the wake of an oscillating airfoil. *AIAA J.* **27**, 1200–1205.

Sarkar, S. & Venkatraman, K. 2006 Numerical simulation of thrust generating flow past a pitching airfoil. *Computers Fluids* **35**, 16–42.

Singh, N., Aikat, S. & Basu, B. C. 1989 Potential flow calculation for three-dimensional wings and wing-body combination in oscillatory motion. *AIAA J.* **27**, 1665–1666.

Triantafyllou, G., Triantafyllou, M. & Grosenbaugh, M. 1993 Optimal thrust development in oscillating foils with application to fish propulsion. *J. Fluids Struct.* **7**, 205–224.

Tytell, E. D. & Lauder, G. V. 2004 The hydrodynamics of eel swimming i. wake structure. *J. Expl Biol.* **207**, 1825–1841.

Usherwood, J., Hedrick, T., McGowan, C. & Biewener, A. 2005 Dynamic pressure maps for wings and tails of pigeons in slow, flapping flight, and their energetic implications. *J. Expl Biol.* **208**, 355–369.

Williamson, C. H. K. & Roshko, A. 1988 Vortex formation in the wake of an oscillating cylinder. *J. Fluids Struct.* **2**, 355–381.